Icarus 210 (2010) 867–880

Contents lists available at ScienceDirect

Icarus

journal homepage: www.elsevier.com/locate/icarus

Investigation of the force balance in the Titan ionosphere: Cassini T5 flyby model/data comparisons

D. Ulusen [a,*], J.G. Luhmann [a], Y.-J. Ma [b], S. Ledvina [a], T.E. Cravens [c], K. Mandt [d], J.H. Waite [d], J.-E. Wahlund [e]

[a] Space Sciences Laboratory, University of California, Berkeley, CA 94720, USA
[b] Institute of Geophysics and Planetary Physics, University of California, Los Angeles, CA 90025, USA
[c] Dept. of Physics and Astronomy, University of Kansas, Lawrence, KS 66045, USA
[d] Southwest Research Institute, 6220 Culebra Rd., P.O. Drawer 28510, San Antonio, TX 78284, USA
[e] Swedish Institute of Space Physics, Box 537, SE-751 21 Uppsala, Sweden

ARTICLE INFO

Article history:
Received 5 April 2010
Revised 19 June 2010
Accepted 5 July 2010
Available online 14 July 2010

Keywords:
Titan
Saturn, Satellites
Ionospheres

ABSTRACT

Cassini's Titan flyby on 16 April, 2005 (T5) is the only encounter when the two main ionizing sources of the moon's atmosphere, solar radiation and corotating plasma, align almost anti-parallel. In this paper a single-fluid multi-species 3D MHD model of the magnetospheric plasma interaction for T5 conditions is analyzed. Model results are compared to observations to investigate the ionospheric dynamics at Titan as well as to understand the deviations from a typical solar wind interaction, such as Venus' interaction with the solar wind. Model results suggest that for the T5 interaction configuration, corotating plasma is the dominant driver determining the global interaction features at high altitudes. In the lower ionosphere below ~1500 km altitude – where the control of the ionospheric composition transfers from dynamic to chemical processes – magnetic and thermal pressure gradients oppose each other locally, complicating the ionospheric dynamics. Model results also imply that the nightside ionosphere – produced only by the impact ionization in the model – does not provide enough thermal pressure to balance the incident plasma dynamic pressure. As a result, the induced magnetic barrier penetrates into the ionosphere by plasma convection down to ~1000 km altitude and by magnetic diffusion below this altitude. Moreover, strong horizontal drag forces due to ion-neutral collisions and comparable drag forces estimated from possible neutral winds in the lower ionosphere below ~1400 km altitude oppose over local regions, implying that the Titan interaction must be treated as a 3D problem. Ion and electron densities calculated from the model generally agree with the Cassini Ion Neutral Mass Spectrometer and Langmuir probe measurements; however, there are significant differences between the calculated and measured magnetic fields. We discuss possible explanations for the discrepancy in the magnetic field predictions.

1. Introduction

Since the 1980s it has been known from Voyager 1 measurements that Titan has a substantial atmosphere and lacks an appreciable intrinsic magnetic field (Hartle et al., 1982; Ness et al., 1982; Bird et al., 1997; Nagy and Cravens, 1998). Orbiting at around 20 saturnian radii distance and therefore remaining inside Saturn's magnetosphere most of the time, Titan mainly interacts with the Saturn's magnetospheric plasma, and only rarely encounters solar wind plasma. Its interaction is expected to be very similar to an unmagnetized planet interaction with a subsonic plasma flow (Ness et al., 1982). Magnetospheric particle impact ionization contributes to the production of the ionosphere, however the major ionization source of the ionosphere globally is solar radiation and the related photoelectron impact ionization (Keller et al., 1992; Nagy and Cravens, 1998; Robertson et al., 2009; Cravens et al., 2009b). The variation of the angle between the solar radiation and corotating magnetospheric plasma due to Titan's motion around Saturn complicates the nature of the interaction making the ionosphere difficult to analyze. In addition to this complex geometry, intricate ion-neutral chemistry makes the governing ionospheric dynamics even more difficult to understand thoroughly (Fox and Yelle, 1997; Keller et al., 1998; Nagy and Cravens, 1998; Cravens et al., 2010; Sittler et al., 2009; Rymer et al., 2009; Bertucci et al., 2009; Simon et al., 2010).

Since the insertion of the Cassini spacecraft into orbit on 1 July 2004, an extensive database describing the saturnian system has been collected. In anticipation of these observations and exploration of the Titan interaction several models – varying from simple 1D ionospheric models to complex 3D hybrid, MHD or empirical models – have been developed (Ip, 1990; Keller et al., 1994; Keller and Cravens, 1994; Cravens et al., 1998, 2009b; Ledvina and Cravens, 1998; Kabin et al., 1999, 2000; Brecht et al., 2000; Nagy

* Corresponding author.
E-mail addresses: demet@ssl.berkeley.edu, demetulusen@gmail.com (D. Ulusen).

0019-1035/$ - see front matter © 2010 Elsevier Inc. All rights reserved.
doi:10.1016/j.icarus.2010.07.004

et al., 2001; Ma et al., 2004a, 2006; Backes et al., 2005; Modolo et al., 2007; Sittler et al., 2009; Simon et al., 2006; Simon and Motschmann, 2009). Analysis of the observations and model results has helped us to understand the global characteristics of Titan's interaction. This global interaction picture is as expected for a slow magnetospheric plasma interaction with an unmagnetized obstacle. Upstream of the moon, magnetic field piles up and downward plasma motion carries magnetic flux into the ionosphere. However, due to time dependent upstream conditions and the often asymmetric relative positions of the sources of atmospheric ionization at Titan, this interaction becomes especially complicated in the lower ionosphere. The relative importance of different forces in the ionosphere, which determines both ionospheric dynamics and magnetic field structure, is still not well understood. Many of the models listed above, such as the 1–2D, empirical or hybrid models, are not capable of providing a sufficiently detailed ionospheric picture due to neglect of the third dimension, unrealistic ionospheric chemistry, or poor spatial resolution.

In this study, we attempt to understand Titan interaction and ionosphere in more detail by analyzing the simulation results from a single-fluid multi-species 3D MHD model run for T5 conditions, and comparing the model predictions to the Cassini Ion Neutral Mass Spectrometer (INMS) (Waite et al., 2004), Radio and Plasma Wave Science – Langmuir probe (RPWS/LP) (Gurnett et al., 2004) and magnetometer (MAG) (Dougherty et al., 2004) observations. Our approach in this study differs from previous model-measurement comparisons for Titan in that we provide an in-depth analysis of the results at low altitudes in the ionosphere rather than making global scale comparisons. We calculate the pressures from different sources in the ionosphere; analyze force balance by calculating force components in the momentum transfer equation and explore the origins of the differences between the model calculations and actual measurements. We chose the T5 flyby for such an analysis as it is a unique encounter having a geometry different from typical solar wind interaction orientations that are well represented by earlier MHD models for Venus and Mars. We compare T5 simulation results to the known features of Venus' interaction to explore the deviations from the classical unmagnetized planet solar wind interactions. (Detailed reviews of the Venus interaction can be found in the Venus 1–2 books by the University of Arizona Press.)

This study is also complementary to recent work by Cravens et al. (2010), where an empirical approach is taken to explore the ionospheric dynamics in Titan's ionosphere. In their work, estimates for thermal and magnetic pressures, plasma flow speeds and time constants of different ionospheric processes are obtained by using Cassini data for the T17, T18, and T5 flybys and by estimating pressure gradients using characteristic length-scales. In this paper, we compare the 3D global MHD description of the Titan interaction to these empirical calculations which are approximated from along-track satellite observations. The consistency between the model and empirical predictions provides a more complete interpretation of both the model results and satellite observations. However, it is understood that the MHD approach is not fully valid for the regions where the ion gyroradius is comparable to the characteristic length scale of the Titan interaction system and randomizing collisions are absent. We expect that the MHD model describes the Titan interaction features more accurately below the region where magnetic field piles up and plasma flow slows down resulting in a significant decrease in the ion gyroradius and below the exobase where collisions dominate. In addition, from previous ideal MHD calculations for Mars, it has been found that the MHD approach is successful in general even in the case of large gyroradius, probably because of the significant wave activity in the vicinity of the obstacle, which acts as pseudo-collisions (Nagy et al., 2001; Ma et al., 2004b).

In this paper, Section 2 presents the Cassini orbit geometry and data for the T5 flyby. Section 3 briefly describes the MHD model, the results of which are analyzed in this study. Section 4 presents the comparisons of the observations with the model predictions. Section 5 includes detailed analysis of the model results in order to understand the governing forces in Titan's ionosphere. Section 6 includes a discussion of our interpretation of the comparison results and Section 7 provides a brief summary.

2. Data summary

In this paper, we used measurements obtained by Cassini during T5 of ion and neutral densities from INMS (Waite et al., 2004; Cravens et al., 2006, 2008; Magee et al., 2009; Cui et al., 2009), electron temperature and density from RPWS (Wahlund et al., 2005; Agren et al., 2007) and vector magnetic field from MAG (Dougherty et al., 2004). The INMS total ion density measurements agree well with the RPWS electron density measurements between ~1000 and 1500 km altitude, where the RPWS density errors are in ~10% and the INMS calibration is accurate to 20% for $M/Z < 50$ daltons and 50% at M/Z of 50 daltons or higher (Agren et al., 2007; Cravens et al., 2006). Below 1000 km altitude, the contribution of the heavier ion species that are not detected by the INMS to the total density is significant (Cravens et al., 2006; Crary et al., 2009). The MAG instrument is capable of determining the absolute magnitude of the field to an accuracy of 1 nT (Dougherty et al., 2004). RPWS and MAG data are available during the entire closest approach (CA) while INMS data are available for only the outbound leg.

In Fig. 1, the portion of the T5 trajectory that remains below 3000 km altitude is shown in the Titan Interaction System (TIIS). (In TIIS, the x axis is aligned with the direction of ideal corotation. The y axis points towards Saturn in Titan's orbital plane. The z axis completes the right-hand system. TIIS is used in all figures throughout the paper.) During T5, Titan was inside Saturn's magnetosphere at 5.3 h Saturn local time. The summary of the geometrical information of T5 is listed in Table 1. The data are presented as time series in Figs. 2 and 3. Even though the behavior at the extremes of the magnetic field plot (Fig. 3) indicates some time-dependence of the magnetospheric conditions at the time of the T5 flyby, this case is one of the more arguably steady cases. Nevertheless, it should be pointed out that Titan was in Saturn's disk plasmasheet during this time and the external magnetospheric particles fluxes probably exceed typical values, especially from the energetic particle measurements at the time (Cravens et al.,

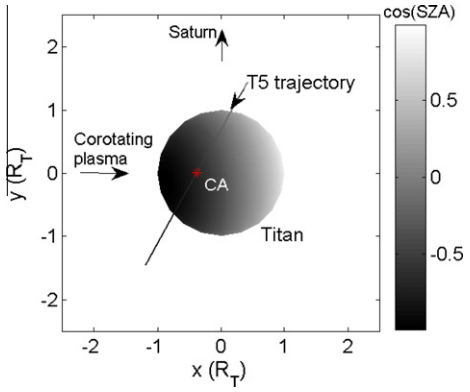

Fig. 1. T5 flyby geometry in the TIIS system. Color scale shows the cos(SZA) over the surface of Titan, ranging from −1 (black) to 1 (white). The red star on the trajectory marks the location of the closest approach (CA) for this pass. (For interpretation of the references to color in this figure legend, the reader is referred to the web version of this article.)

Table 1
Trajectory parameters and observational data for T5.

Date	16 April, 2005
CA altitude	1025 km
Titan's location in the Saturn system	5.3 h Saturn local time
Subsolar location on Titan	170° from the subram point, −22° from the Titan–Saturn plane
SZA range	From 88° to 143°
Pass description	A nightside corotation ram face pass

2008; Rymer et al., 2009), that the magnetosphere was producing a higher than average energetic particle environment for Titan.

3. Model summary

Only a brief overview of the 3D MHD simulation of the plasma interaction during T5 is given here; details can be found in Ma et al. (2006). In this model, the complex chemistry of Titan is approximated by seven representative ion species (listed in Table 2) and 10 background neutrals (N_2, CH_4, H&H_2, C_2H_2, C_2H_4, C_2H_6, C_3H_4, C_4H_2, HCN, HC_3N). The mass densities of each ion species are tracked using seven continuity equations taking into account photoionization, impact ionization, charge exchange, and recombination. The rate of each process is determined by combining appropriate reactions from a detailed 51 ion species chemical equilibrium model described by Keller et al. (1998) and Cravens et al. (2005). A number of these reaction rates are temperature dependent (Schunk and Nagy, 2000) and required electron temperatures are adopted from Gan et al. (1992).

The main source of ionization in the dayside ionosphere of Titan is solar radiation (Agren et al., 2009; Robertson et al., 2009). In the model, ion production calculations associated with this source consider SZA and altitude dependencies. Secondary ionization due to superthermal electrons created during photoionization is also included in the calculations, which is important at lower altitudes. The impact of the corotating magnetospheric plasma with the Titan atmosphere is another source of ionization having only altitude dependency and contributing to both dayside and nightside ionosphere (Crary et al., 2009; Sittler et al., 2009; Cravens et al., 2009a). The incident magnetospheric plasma is assumed to consist of superthermal electrons, oxygen (O^+), and hydrogen (H^+) ions represented by Maxwellian distributions (parameters are listed in Table 3) (Crary et al., 2009; Agren et al., 2007, 2009; Cravens et al., 2008). It is also thought that energetic ion precipitation may also play a role (Cravens et al., 2008), but mainly at altitudes below 1000 km.

In the model, neutral densities are adopted from Yung et al. (1984), Yung (1987) and Keller et al. (1992), which are independent of local time and latitude. Both neutral and newly produced ion temperatures are taken to be 150 K (from Cassini INMS measurements, Waite et al. 2005). Furthermore, the velocity and temperature of all ion species are assumed to be equal, which simplifies the seven momentum equations to a single equation. At Titan the electrical conductivity of the plasma is high on the dayside and at high altitudes where magnetic diffusion can be neglected. However on the nightside and at lower altitudes the plasma is weakly ionized, making collisions important and increasing the resistivity of the plasma. Over these regions, magnetic diffusion cannot be ignored and the electrical conductivity of the plasma is calculated considering the collisions between electrons and three major neutrals (N_2, CH_4, H_2). In these calculations, collision frequencies are adopted from Keller et al. (1992), and electron temperature is calculated from the plasma temperature. In previous studies of Ma et al. (2006, 2007), comparisons of model plasma densities with chemical equilibrium model results show good agreement, confirming that the detailed 51-species chemical model is well represented by the simplified seven-species model. The differences at high altitudes (>1400 km) imply the importance of plasma transport at these altitudes.

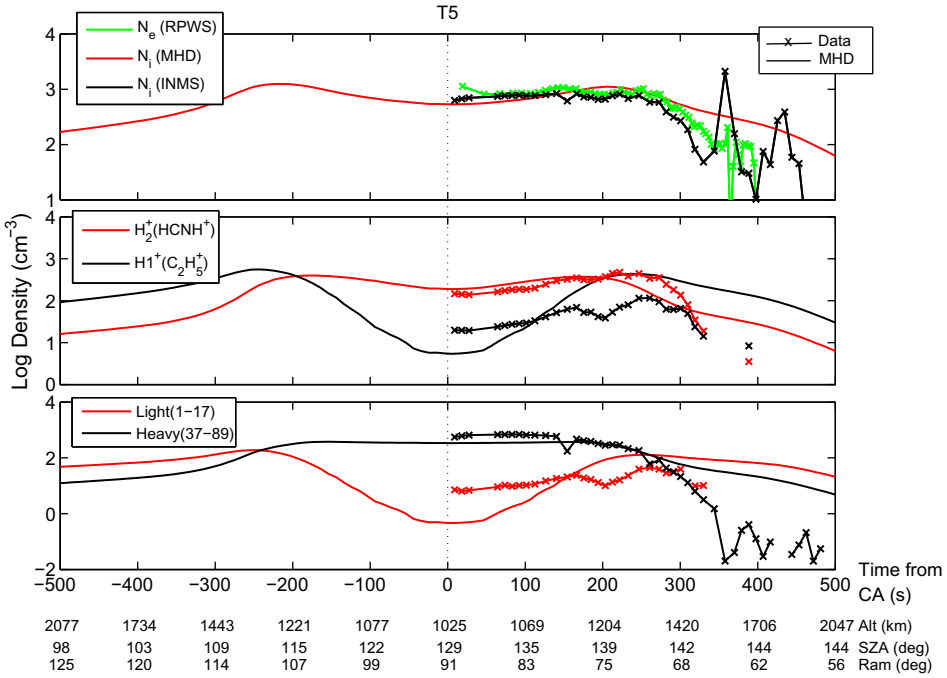

Fig. 2. Comparison of ion densities obtained from INMS data, total electron density from RPWS data and model calculations. The densities are plotted on a log scale as a function of time in seconds from CA. Solid lines represent the model predictions and the solid lines with symbols represent the observations. Each color indicates different species. Top panel compares total ion and electron, middle panel compares the most abundant ion species ($HCNH^+$ and $C_2H_5^+$) and bottom panel compares light (L^+ and M^+ (1–17)) and heavy (MHC^+, HHC^+, HNI^+ (37–89)) ion species from the model calculations to the satellite measurements. (For interpretation of the references to color in this figure legend, the reader is referred to the web version of this article.)

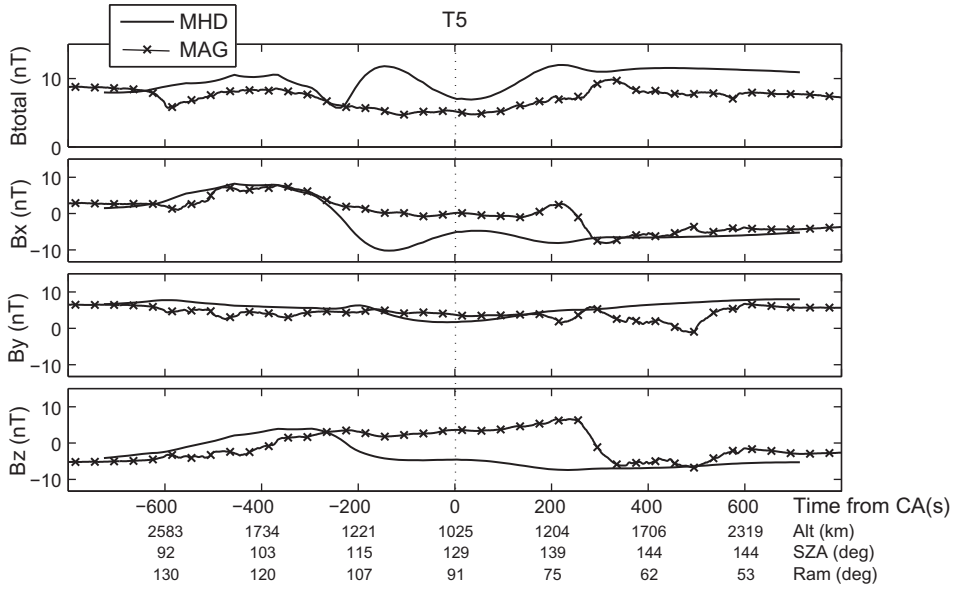

Fig. 3. Comparison of magnetic field components obtained from MAG instrument and model calculations along T5. Field strengths are plotted in nT as a function of time in seconds from CA. Solid lines show MHD results while solid lines with symbols show actual data. The first panel compares the total field while the bottom three panels compare *x*, *y*, *z* components in TIIS system.

Table 2
Seven representative ion species used in the MHD model.

Name	Components	Mass (amu)	Mass range (amu)
L^+	H_1^+, H_2^+, H_3^+	1	1–3
M^+	CH_5^+, N^+, CH_4^+, CH_3^+, CH_2^+, CH^+, C^+	14	12–17
H_1^+	$C_2H_5^+$	29	29
H_2^+	$HCNH^+$	28	28
MHC^+	C_3H^+, $C_3H_2^+$, $C_3H_3^+$, $C_3H_4^+$, $C_3H_5^+$, $C_4H_3^+$, $C_4H_5^+$,...	44	37–53
HHC^+	$C_5H_3^+$, $C_5H_5^+$, $C_5H_7^+$, $C_5H_9^+$, $C_6H_5^+$, $C_6H_7^+$, $C_7H_5^+$,...	70	63–89
HNI^+	$C_3H_2N^+$, $C_5H_5N^+$, C_3HN^+	74	51–79

Table 3
Model parameter values used in the runs for T5.

N(e)	0.1 cm^{-3}
$N(O^+)$	0.1 cm^{-3}
$N(H^+)$	0.05 cm^{-3}
U (TIIS)	(120, 0, 0) km/s
T (Ti=Te)	1000 eV
B (TIIS)	(2.0, 5.5, −3.5) nT, B_{mag} = 6.8 nT
Subsolar location on Titan (TIIS)	(0.911, 0.169, −0.3744)

The model equations are solved using the BATRUS code (Powell et al., 1999). In the calculations a spherical grid system in the TIIS system is used which provides a good radial resolution in the ionospheric region. The highest resolution is ~35 km near the obstacle boundary; an absorbing sphere for velocity and magnetic field located at 725 km (=0.28 in Titan radius) altitude above the surface of Titan (absorbing boundary for velocity and magnetic field forces them to have zero gradients at the inner boundary and lets the field lines penetrate into the obstacle surface). Angular resolution is 2.5° in both azimuthal and latitudinal directions. At the inner boundary, the ion densities were set at their chemical equilibrium values. The summary of the upstream parameters determined from the Cassini observations for T5 is given in Table 3. Equal ion and electron temperatures, Ti=Te, are assumed although the actual ratio of the temperatures between electron and ions varies with time and location at Titan.

4. Simulation results and comparisons with observations

In Fig. 2, densities of ion species from the model are compared with the Cassini measurements near CA during T5. Densities are plotted on a logarithmic scale as a function of time in seconds from CA. Solid lines represent the model results and solid lines with symbols represent measured values. Since, only outbound INMS data are available for T5, the lines for INMS do not extend to negative times. In the first panel, total ion densities from the model results are compared to INMS total ion and RPWS total electron measurements. Between 1000 and 1500 km, the INMS measurements agree well with the RPWS electron densities, where the error bars for RPWS electron densities are ~10% (Agren et al., 2007; Cravens et al., 2006, 2008) and in the same altitude range model results fit well with the observations. Between these altitudes, the model predicts the location of the ionospheric peak correctly (~1200 km – note that there is not a sharp electron density peak for T5 but more of a ledge) but with a slightly higher peak density (model = 1.1×10^3 cm^{-3}; RPWS = 10^3 cm^{-3}; INMS = 0.8×10^3 cm^{-3}). Above 1500 km, the model predictions are higher than the RPWS electron measurements and the deviation between the model and actual data increases substantially as the altitude increases. But from this comparison we can say that in general model predictions show a reasonable agreement with the observations in the dense ionosphere below 1500 km which demonstrates that the model has a reasonable balance between ion sources and sinks, at least for the major ion species. In the second panel the densities of the most

abundant ion species from the model are compared to INMS observations. As seen in this plot, while $HCNH^+$ is well represented by the model, $C_2H_5^+$ is underestimated at low altitudes and overestimated at high altitudes. This behavior is similar to what we observe for the heavy and light ion comparisons in the bottom panel. While the model represents heavy masses (MHC^+, HHC^+, HNI^+ (37–89)) well, light masses (L^+ and M^+ (1–17)) are underestimated at low altitudes and overestimated at high altitudes. The differences in the ion densities can result from many factors including the simplified description of the atmospheric/ionospheric chemistry, incorrect neutral abundance profiles, uncertainties in the upstream parameters used in the model, MHD model approximations as well as temporal variations and instrumental errors.

Fig. 3 compares the magnetic fields obtained from the model and MAG instrument near CA during T5. Field strengths (in units of nT) are plotted as a function of time (in units of seconds) from CA. The top panel shows the comparison of the total field while the bottom three panels show the comparisons of TIIS *x*, *y*, and *z* components, respectively. As seen in these plots, the observed magnetic field exhibits variations ranging from −10 to 10 nT and the order of the field strengths predicted by the model is close to the observations with the model field strength being somewhat higher than the measurements on the outbound trajectory; however, detailed field components do not match the data as well as the ion densities. Deviations between the data and model predictions are more detectable near CA, especially during the 600 s centered on CA. This time period corresponds to a region in Titan's ionosphere below 1500 km altitude, which is roughly where the plasma transport due to many different sources may be effective. A more detailed discussion of the reason for this discrepancy between the calculated and observed magnetic field is included in Section 6.

Although the present model does not reproduce the detailed variations in the magnetic field observations very effectively, the analysis of the model results is still useful for understanding the ionospheric dynamics at Titan. Unlike Venus, the substantial thickness of Titan's ionosphere and potential horizontal forces and horizontal plasma motion, especially in the region below the exobase (∼1500 km) – as suggested by Cravens et al. (2010), Müller-Wodarg et al. (2008), and Cui et al. (2009) – imply that modeling Titan's interaction and ionosphere requires a 3D treatment. Therefore, 3D numerical experiments such as the one presented here are necessary for analysis of Titan's ionosphere. Understanding the discrepancy seen between the observed and calculated magnetic fields may help reveal the relative importance of different ionospheric forces and MHD theory limitations, as well as provide insight for future modeling attempts. A third reason is that T5 is the only encounter where the hemispheres dominated by the two main ionizing sources of the moon's atmosphere, solar radiation and magnetospheric impact, are well-separated, i.e., solar induced ionosphere on the corotation wake side while the main magnetospheric interaction is on the corotation ram/nightside. This geometry is different from typical solar wind interaction orientations that are well represented by earlier MHD models, making T5 particularly interesting and important for understanding the differences from non-magnetized planet interactions with the solar wind.

5. Model analysis

Under T5 conditions the main field pileup is expected to take place on the nightside of Titan and the simulation results obtained for T5 are consistent with these expectations. In two rows in Fig. 4,

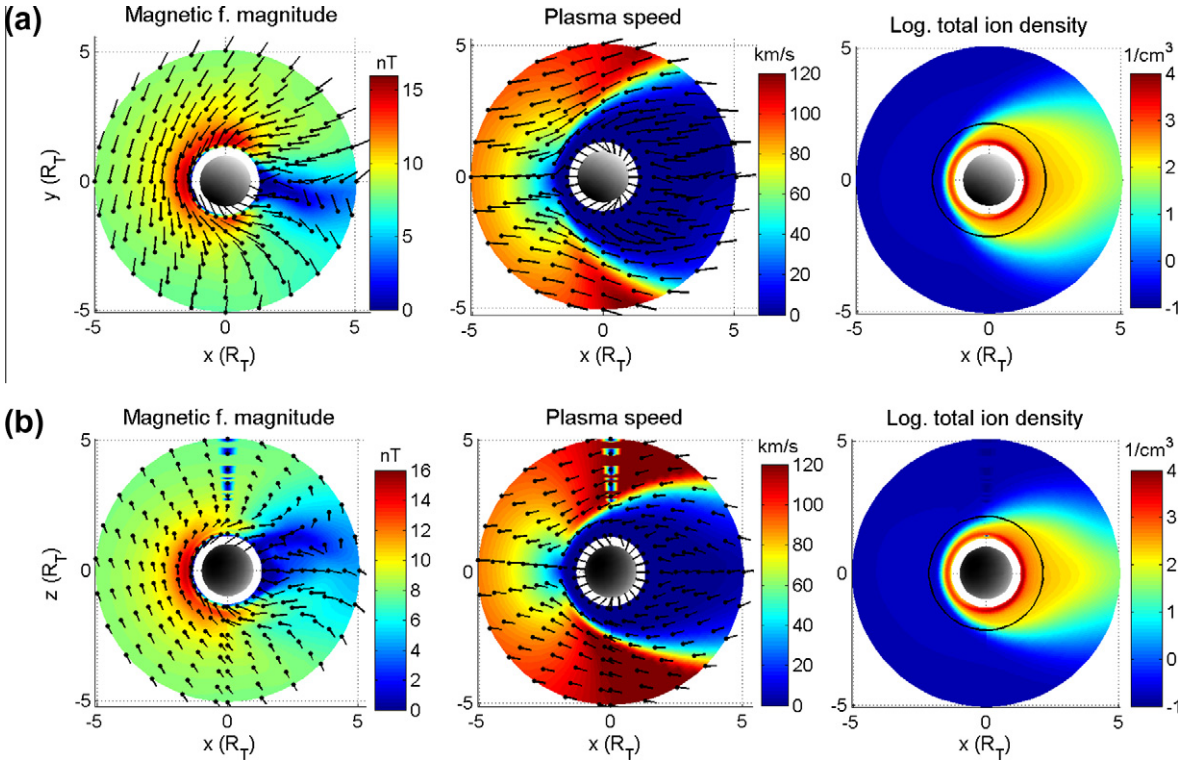

Fig. 4. (a and b) Contours of the magnetic field magnitude (B) in nT, plasma speed (*U*) in km/s, and total ion density *N*(ion)(1/cm^3) on a log scale obtained from T5 simulation are plotted in the *xy* and *xz* planes. Distance is scaled in Titan radius (R_T = 2575 km). Solar illumination is indicated by the gray color scale (similar to Fig. 1) which shows cos(SZA) over the surface of Titan, ranging from −1 (black) to 1 (white) (for brevity colorbar is not shown, one can refer to Fig. 1 for the gray color scale). At low altitudes white area denote the regions inside the model boundary but above the planet. (For interpretation of the references to color in this figure legend, the reader is referred to the web version of this article.)

contours of the magnetic field magnitude, plasma flow speed, and ion density are shown in the *xy* and *xz* planes, respectively. On the magnetic field and speed contours, the normalized magnetic field and velocity vectors are projected (black lines with dots at one end) and the starting point of each vector is indicated by a black dot. In the magnetic field plots (the first column of figures in Fig. 4), the piling up and draping of the magnetic field in the upstream region and the two-lobe induced tail structure downstream of the corotating plasma flow is evident. The asymmetry seen in the magnetic field is the result of the tilted upstream magnetic field used in the model. The magnetic field reaches its maximum of 16.4 nT at 1180 km altitude near 175°E, 95°S and drops to almost zero at around 900 km altitude. In the velocity figures (the second column of figures in Fig. 4), ideal plasma corotation direction (−12,000 km/s) assumed in the model calculations is evident from the vector plots. As seen in these figures, without an observable bow shock formation, magnetospheric plasma gradually slows down in the vicinity of Titan due to mass loading by the atmosphere ion production. Along the plasma corotation direction, the flow speed gradually drops from 120 to 40 km/s between several Titan radii and 2500 km altitude; and then sharply drops from 40 km/s to tens of m/s between 2500 and 1500 km altitudes. Below about 2000 km, these flow speeds are approximately the same as Cravens et al.'s (2010) empirical estimates. In the last column of panels in Fig. 4, the total ion density distribution shows the dominant effect of the solar radiation on the dayside. The peak density is 6300 cm^{-3} at 1110 km altitude along the subsolar line. A less populated broader ionosphere forms on the nightside due to impact ionization as described in the previous section, with a peak density of 4000 cm^{-3} at 1220 km altitude. These peak densities and altitudes for the dayside and nightside ionospheres are in the typical ranges observed at Titan by RPWS and presented by Agren et al. (2009).

Pileup of the magnetic field on the nightside and existence of a denser ionosphere on the wake side is the main difference in the Titan interaction under T5 conditions from a typical non-magnetized body–solar wind interaction, such as the Venus interaction, where solar radiation and wind flow directions coincide. Although the main source of this nightside ionization is assumed to be magnetospheric electron impact at Titan, a significant contribution of the cross-terminator plasma transport as at Venus is possible (Brace et al., 1990; Brace and Kliore, 1991; Cui et al., 2009). (Note that this model should have both the *in situ* and transport sources since it does have some seven-species ion chemistry.) In the next section we will address this question as well as some others associated with the ionospheric dynamics by taking a closer look at the pressure and force balance in the ionosphere, analyzing the altitude profiles at different locations in the Titan interaction geometry and comparing these to known features of the Venus interaction. However before that we describe the background for our analysis, the MHD momentum equation:

$$\rho\left(\frac{\partial \mathbf{u}}{\partial t}+\mathbf{u}\cdot\nabla\mathbf{u}\right)=-\nabla(p_e+p_i)+\mathbf{J}\times\mathbf{B}+\rho\mathbf{g}+\rho\nu_{in}(\mathbf{u}_n-\mathbf{u}) \qquad (1)$$

In the present model, a single momentum transfer equation (Eq. (1)) is solved to establish the force balance, assuming all ions have the same temperature and velocity. In Eq. (1), ρ is ion mass density, $\mathbf{u}$ is single-fluid ion velocity, p_e and p_i are electron and ion thermal pressures ($p_j = n_j k T_j$), respectively, where n_j is number density of species 'j' and T_j is kinetic temperature, $\mathbf{J}$ is current density, $\mathbf{g}$ is the gravitational acceleration, ν_{in} is the collision frequency between the neutral gas 'n' and ions 'i', $\mathbf{u}_n$ the neutral velocity. The simulation begins with initial out-of-balance conditions and converges on a quasi-steady solution as long as the external conditions are constant.

Each component in Eq. (1) corresponds to a different force component in Titan's ionosphere. Starting from the right hand side, the first term is the thermal pressure gradient force; the second term is the magnetic force; the third term is gravitational acceleration; and the last term is the drag force. The magnetic force can often be approximated by the magnetic pressure gradient force as the curvature tension force is usually negligible in the ionosphere, but the numerical MHD model has the full $\mathbf{J}\times\mathbf{B}$ force. Furthermore, in the present model, neutral winds are ignored, reducing the drag force term to $\rho\nu_{in}\mathbf{u}$. If we further assume steady state and slow ionospheric plasma flow in the lower ionosphere, we can also ignore the inertial terms on the left hand side and reduce Eqs. (1) and (2).

$$0=-\nabla(p_e+p_i)-\nabla\left(\frac{B^2}{2\mu_0}\right)+\rho\mathbf{g}-\rho\nu_{in}\mathbf{u} \qquad (2)$$

Eq. (2) amounts to a relatively simple statement of pressure balance. Cravens et al. (2010) solved Eq. (2) for the flow velocity and used approximate length-scales to estimate the pressure gradient terms. In the current paper we will evaluate these terms using the numerical 3D MHD model results.

An even simpler force balance relation is obtained when gravity and ion-neutral collisions can be ignored.

$$0=-\nabla(p_e+p_i)-\nabla\left(\frac{B^2}{2\mu_0}\right) \qquad (3)$$

Utilizing the equations above, in the next sections, we analyze the different pressure components in Titan's ionosphere for the region below 3000 km altitude, which is marked by the black circle shown on the ion density plot in Fig. 4. It will be seen that the vertical pressure balance that is used so effectively to describe the solar wind interaction at Venus is not as clearly apparent at Titan. We also analyze the various forces that control the ionosphere's response to the plasma interaction.

5.1. Pressure profile diagnostic

Fig. 5a and b shows the magnetic, thermal, and dynamic field pressures in the *xy* and *xz* planes, respectively, below 3000 km altitude. This allows us to indentify the dominant ionospheric forces represented in the model. As seen in these figures, different pressure components are dominant in different regions. Since the angle between the solar and magnetospheric ionization sources is about 170° during T5, magnetic field pressure is dominant on the ram side due to the piling up of the field, and thermal pressure is dominant on the dayside/wake side due to the elevated plasma density associated with photoionization by solar radiation. The slight drop in the magnetic field pressure on the ram side – before it peaks locally and drops to zero near the inner boundary – is due to increase in the balancing nightside ionospheric thermal pressure. This ionospheric pressure increase is evident in the thermal pressure plots (the greenish circular extension of the dayside ionosphere to the nightside). Dynamic pressure is decreased on the ram side mainly because of mass loading. The red regions close to the outside edges of the figure are part of the high dynamic pressure from the corotation flow on the upstream side. A secondary sharp and global drop in the dynamic pressure below ~1500 km altitude (dark blue region) is the result of the effective slow down of the plasma due to the high ion-neutral collision frequency. Therefore, below 1500 km on the ram side, the control of the ionospheric structure changes from dynamical to chemical as transport times exceed chemical lifetimes (Keller et al., 1994; Cravens et al., 2010; Robertson et al., 2009; Ma et al., 2006). On the dayside, above this transition region, relatively high dynamic pressure (ρv^2) at the flanks in the

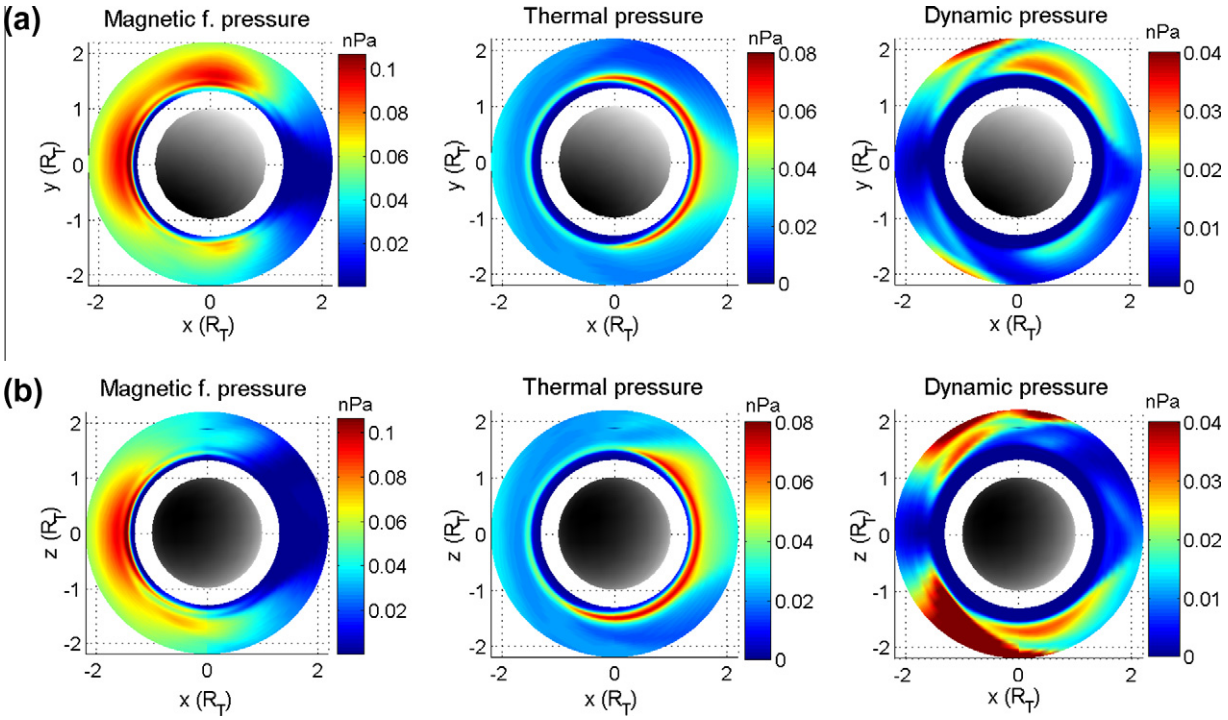

Fig. 5. (a and b) Contours of the magnetic field (PB), thermal (PT), and dynamic (PD) pressures in nPa obtained from T5 simulations are plotted in the *xy* and *xz* planes in the Titan's ionosphere (below 3000 km altitude). Solar illumination is indicated by the color scale which shows cos(SZA) over the surface of Titan, ranging from −1 (black) to 1 (white) (for brevity colorbar is not shown, one can refer to Fig. 1 for the gray color scale). At low altitudes white area denote the regions inside the model boundary but above the planet. (For interpretation of the references to color in this figure legend, the reader is referred to the web version of this article.)

xy plane and at the −*z* flank in the *xz* plane are observed because, over these regions, ionospheric plasma density and plasma speeds are relatively higher than in the neighboring regions.

The major ionization source of Titan's dayside ionosphere is solar radiation and the related photoelectron impact ionization; however, the main source of Titan's nightside ionosphere is still a debated subject, just as it was for Venus in 1980 or so (Cravens et al., 2009a). While in their models Cravens et al. (2008) and Agren et al. (2007) reproduced the measured densities on the nightside (for T5 and T21) using only *in situ* magnetospheric electron impact ionization, by analyzing the averages from a set of INMS ion density measurements Cui et al. (2009) argued that day-to-night transport of the chemically long lived species also contributes to the nightside ionosphere. At Venus under solar maximum conditions, the ionopause is located at high altitudes and a cross-terminator plasma flow sustains most of the nightside ionosphere. However at Venus solar minimum, when the ionopause is moved to lower altitudes, such day-to-night transport stops and the local plasma

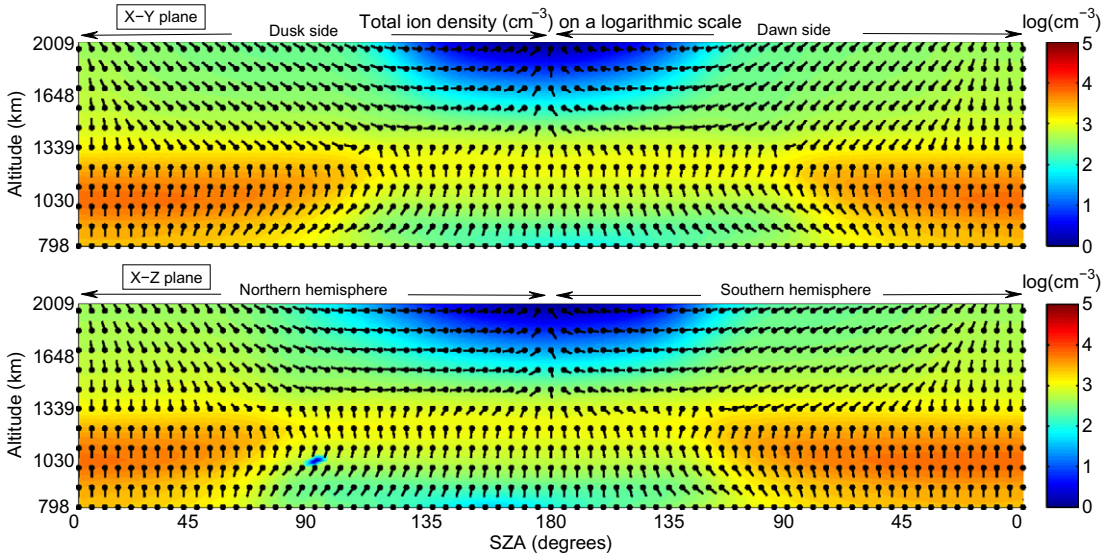

Fig. 6. Contours of the total ion density obtained from the model results in the *xy* and *xz* planes, plotted as a function of altitude vs. SZA. Color scale indicates the total ion density on a logarithmic scale and black lines with dots represent the normalized flow vectors projected on the corresponding plane. The dots on the lines indicate the starting point of the vectors.

precipitation remains the only source (Knudsen et al., 1980; Cravens et al., 1983; Luhmann and Cravens, 1991). Also at Venus, the main ion being transported nightward is the atomic species, O^+, which does not readily recombine, whereas at Titan the longer-lived species are molecular ion species.

In Fig. 6, we explore the nature of the cross-terminator plasma flow from day to night in the model predictions under T5 conditions. In this figure, the total ion densities shown in the *xy* and *xz* planes are color mapped and plotted as a function of altitude and SZA. The black lines with dots represent the normalized flow vectors projected in the corresponding planes and the dots on the lines indicate the starting point of the vectors. The asymmetry in the density distributions in both planes is due to the fact that the angle between the Sun–Titan line and the *xy* and *xz* planes are −20° and 10°, respectively. A denser and broader dayside ionosphere is apparent at lower solar zenith angles (i.e., closer to the subsolar point), and relatively less dense and narrower nightside ionosphere with higher peak altitudes is evident near the center of both planes (where the SZA is close to 180°). As seen in the flow vectors, corotating plasma approaches the body on the nightside and deviates around the moon at lower SZAs. Just above the dayside ionospheric peak there is a clear boundary above which the flow moves upward and below which the flow moves downward. This boundary is located higher at the flanks. At the two edges of the dayside ionosphere in both planes (at the boundary of the reddish regions along ~90 SZA where there is a transition from day to nightside ionospheres), there is a weak cross-terminator plasma flow at around 1200 km altitude, likely deriving from the thermal pressure gradients. However the direction of this flow reverses from day-to-night to night-to-day at lower altitudes along the same SZAs. Therefore, under T5 conditions, the model results imply that such a day-to-night transport is minimum if not zero as the magnetic and thermal pressure gradients oppose for T5 and the nightside ionosphere is produced mostly by the *in situ* magnetospheric electron impact mechanism. A noticeable day-to-night transport, as suggested by Cui et al. (2009) especially below ~1400 km, would be more likely to occur when the magnetospheric flow and solar radiation align as in the Venus case.

For a more detailed analysis of the pressure distributions around Titan, pressure altitude profiles are sampled along ram, +*y* ram–flank, −*y* ram–flank, and anti-ram directions in Fig. 7a while profiles sampled along the subsolar, +*y* terminator, −*y* terminator, and anti-solar directions are plotted in Fig. 7b. The similarity between the ram and anti-solar profiles; terminator and flank profiles; anti-ram and subsolar profiles are evident in these figures, which is expected as subsolar and subcorotation hemispheres are almost opposite during T5. As seen in the ram (anti-solar) profiles, there is a point at ~7000 km where collisions are negligible and all pressure components are comparable. Above this altitude, dynamic pressure is effective, and below this altitude both magnetic and

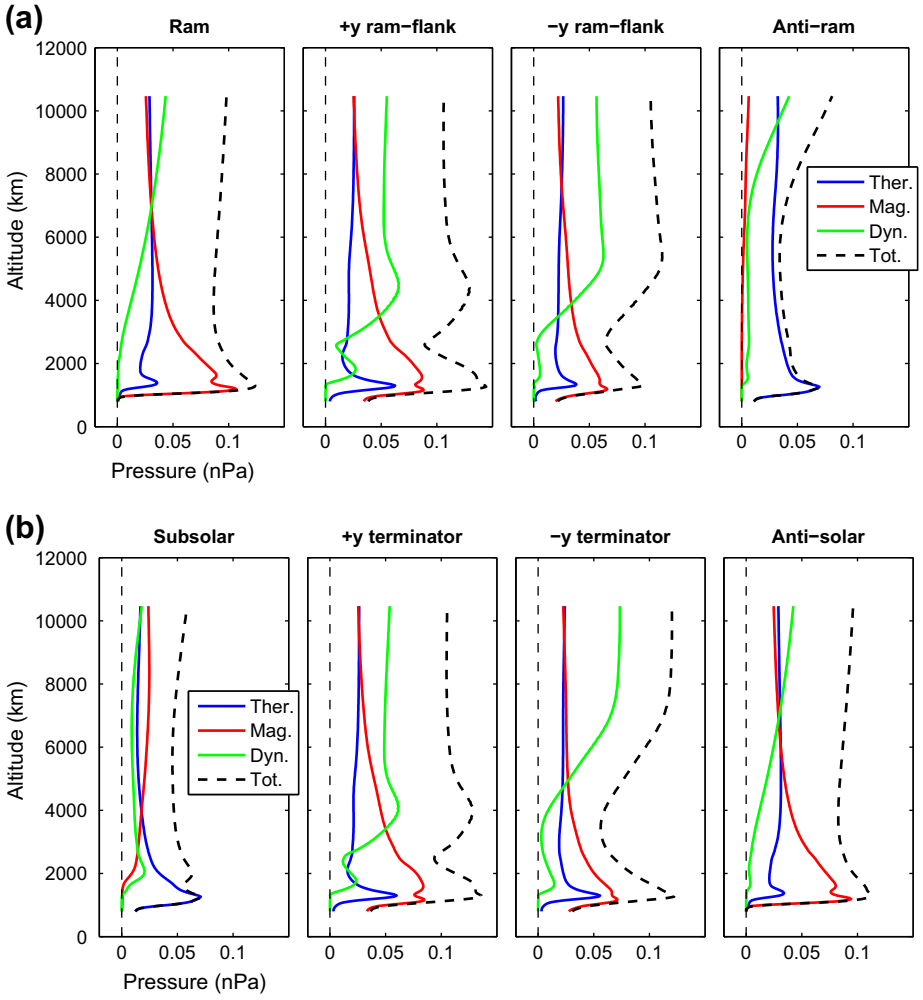

Fig. 7. (a and b) Altitude profiles of thermal (blue), magnetic (red), dynamic (green), and total (dashed black) pressures obtained form T5 simulation results along ram, +*y* ram-flank, +*y* ram-flank and anti-ram directions and along subsolar, +*y* subsolar-terminator, −*y* subsolar-terminator and anti-solar directions. All pressures are in nPa and altitude is km. (For interpretation of the references to color in this figure legend, the reader is referred to the web version of this article.)

thermal pressure increase and magnetic pile up continues down to the lower ionosphere where magnetic pressure becomes dominant. Although the thermal pressure balances some part of the dynamic pressure at around 1300 km (notice the drop in magnetic field pressures), it is still not enough to balance it entirely. Because of direction of the gradient of the total pressure profile, plasma is forced upward above the total pressure peak (at ~1300 km and downward below it (as mentioned in the previous paragraph). Over the flanks (terminators), total pressure is the highest as the plasma is accelerated by mainly the magnetic tension forces. (Note that for T5 Cassini flew through the ram and ram–flank regions and did not directly observe the subsolar/anti-ram region.)

Another interesting feature in these profiles is the behavior of the magnetic field near the inner boundary: The magnetic field drops to almost zero at low altitudes on the ram side while it remains non-zero over the flanks, having almost equal radial and horizontal components (~10 nT each) above 1100 km altitude and a mostly radial component (~9 nT) below 1100 km (non-zero fields at low altitudes are also apparent in Fig. 4a and d). The presence of the non-zero fields in the lower ionosphere can be explained by the penetration of the magnetic barrier into the ionosphere via plasma convection up to an altitude and beyond this altitude the magnetic diffusion may be the main reason for the non-zero fields (Keller et al., 1994; Cravens et al., 2010). Moreover, the absorbing inner boundary condition – zero magnetic field gradients at the boundary – allows the magnetic fields to penetrate into the obstacle surface leading to non-zero radial fields at the inner boundary over the flanks. The source of these non-zero fields will be discussed in more detail later in this section. As evident in the anti-ram profiles, unlike Venus' nightside wake, during the T5 flyby, Titan's ram wake is on the dayside and extends to several Titan radii where the thermal pressure is dominant, as expected.

These features observed in the ram and flank profiles at Titan are different than the general features of Venus' interaction. At Venus, under solar maximum conditions, on the ram side of the interaction from high to low altitudes, a clear transition is observed from a dominant dynamic pressure to magnetosheath thermal pressure, then to magnetic pressure in the magnetic barrier, and finally to thermal pressure in the ionosphere due to the high plasma densities. In such cases the ionospheric thermal pressure is sufficient to balance the incident solar wind dynamic pressure above the collisional region, leading to a sharp ionopause (Luhmann et al., 1987; Luhmann and Cravens, 1991). However in the nightside ionosphere of Titan, such a transition is not detectable and the thermal pressure is too weak to stand off the dynamic pressure of the corotating plasma. Therefore magnetic pile up continues down to Titan's deep ionosphere which is more like the situation expected in Venus' ionosphere at solar minimum. At Venus under solar minimum conditions the pressure balance altitude generally reaches into the collisional region, resulting in the penetration of magnetic barrier field into the ionosphere by magnetic diffusion (Elphic et al., 1980; Luhmann et al., 1987; Luhmann and Cravens, 1991; Shinagawa and Cravens, 1988).

Model calculations show that at Titan magnetic resistivity becomes significant at ~1000 km. This altitude is the same as Keller et al.'s (1994) and Cravens et al.'s (2010) estimates for the altitude where diffusion starts dominating. Therefore above this altitude magnetic diffusion is less probable and similar to Venus, the non-zero magnetic fields in the lower ionosphere may be due to penetration of the magnetic barrier into the ionosphere by plasma convection down to 1000 km and due to magnetic diffusion below 1000 km altitude (Elphic et al., 1980; Luhmann and Cravens, 1991; Zhang et al., 1991, 2006, 2007). In addition to thermal pressure and ionospheric collisions, stability of the upstream magnetic field is another factor that determines the magnetization of the ionosphere for unmagnetized body interactions. The long term average of the external magnetic field – Saturn's internal magnetic field – is different from zero at Titan favoring magnetization of the ram side ionosphere under the conditions similar to T5.

5.2. Force balance diagnostic

In order to understand the dynamics of Titan's ionosphere, we calculate each force term in Eq. (2) along the ram, ±ram–flank, and anti-ram directions below 1800 km altitude (in nN/m^3) and display these terms in Fig. 8. (As explained in the previous section, due to similarity in the subsolar direction profiles we only plot the force profiles referred to the ram direction.) Radial, longitudinal, and azimuthal components of the forces are plotted in Fig. 8a–c, respectively. For the purpose of comparison, scales are kept the same in all panels. As mentioned in Section 5, in the present model neutral winds are ignored. In order to explore the possible effects of the neutral winds in Titan's ionosphere we non-self-consistently estimated the drag force – ($\rho\nu_{in}\mathbf{u}$) due to possible coupling between the plasma and neutral winds – by utilizing the results of an empirical thermospheric model of Müller-Wodarg et al. (2008).

In this calculation of the drag force, for the plasma mass densities and collision coefficients we used the MHD model calculations (Ma et al., 2006; Keller et al., 1994; Schunk and Nagy, 2000) and for the neutral wind speeds we used averages from the empirical thermospheric model of Müller-Wodarg et al. (2008). We assumed that the vertical, longitudinal, and meridional speeds of the neutral winds in the *xy* plane are 1, 1, and 25 m/s, respectively, between 1000 and 1800 km altitudes. The net force, *Net***F**, and that due to winds $\mathbf{F}_{winds}$ is then:

$$Net\mathbf{F} = -\nabla(p_e + p_i) - \nabla\left(\frac{B^2}{2\mu_0}\right) + \rho\mathbf{g} + \rho\nu_{in}(\mathbf{u}_n - \mathbf{u}) \tag{4}$$

$$\mathbf{F}_{winds} = \rho\nu_{in}\mathbf{u}_n \tag{5}$$

There are four important features of the force profiles shown in Fig. 8. (1) The radial or vertical force components, except the neutral drag force, exceeds the horizontal force components in all directions (ram, ±flank, anti-ram). (2) Drag forces provide the force balance at low altitudes. (3) Although the horizontal (longitudinal and meridional) components of magnetic, thermal and gravity forces (Fig. 8b and c) are small compared to their radial values (Fig. 8a), horizontal drag forces are significant in the flank regions. (4) The azimuthal component of the neutral drag force is stronger than other contributions along all directions (ram, ±flank, anti-ram). Each of these features points to important characteristics of Titan's interaction, but this is because of the neutral wind vector that was adopted. The first feature implies that, similar to the Venus interaction on the dayside, major variations are along the radial direction in Titan's ionosphere.

For T5 conditions, all force components play an important role somewhere in the ionosphere, but in the lower ionosphere (below 1400 km) ram and flank regions the radial magnetic pressure gradient force (red) dominates and is balanced by ion-neutral drag (black). This characteristic is also the result of the second feature which shows the importance of the ion-neutral collisions in the lower ionosphere. Similarly, over the flanks, the combined radial thermal and magnetic force is balanced mainly by the drag force. The third feature implies that horizontal forces and therefore horizontal plasma motions may be important at Titan, especially below 1400 km altitude. Even though our estimates of neutral wind effects are not self-consistent in that they are computed using MHD model results obtained with zero neutral winds, the last feature suggests that neutral wind-ionospheric plasma coupling may alter the magnetic field structure at low altitudes. And this is consistent with the empirical estimates of Cravens et al.

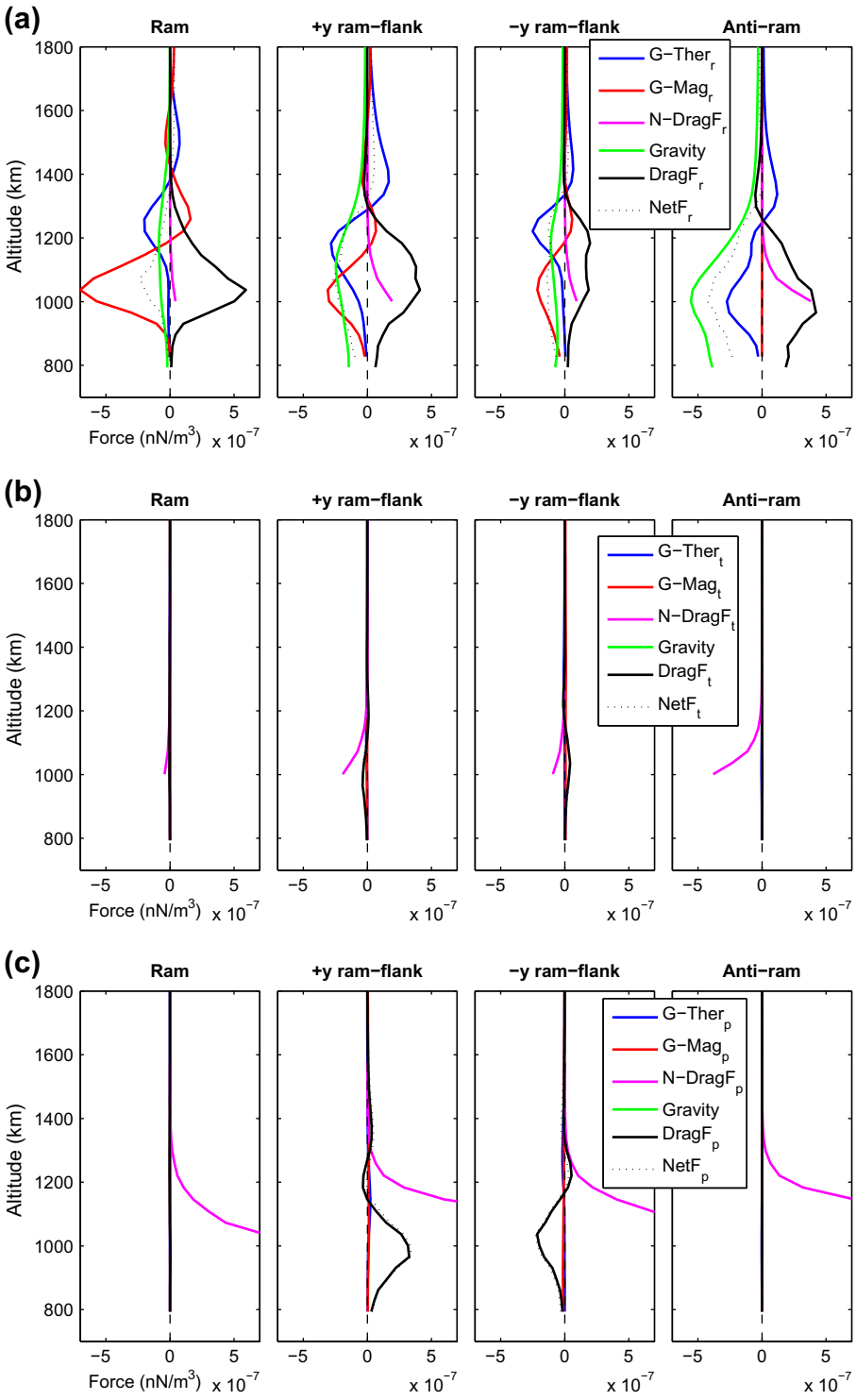

Fig. 8. (a–c) Altitude profiles of each force components in the spherical coordinate system ((a) radial, (b) longitudinal, and (c) azimuthal) calculated form the T5 simulation results along ram, +*y* ram-flank, −*y* ram-flank, and anti-ram directions. Forces are in nN/m^3 and altitude is in km.

(2010). As evident in −*y* ram–flank profiles, opposing neutral wind and plasma drag forces may result in a shear which would then lead to unpredictable magnetic field distributions below 1400 km altitude (also see discussion in Cravens et al. (2010)). Therefore, one reason for the inconsistency between the ion density and magnetic field representations in the MHD model compared to observations may be the exclusion of the neutral wind effects. As explained in the previous paragraph, in the neutral drag force calculations we used the results from Muller-Wodarg et al. (2008); however, as noted by these authors, there are large uncertainties in this value due to unknown forcing from waves and coupling to the lower atmosphere. We therefore also consider wind speeds 10 times smaller and find that the horizontal components of these forces are still comparable to other ionospheric forces and our conclusions about the last feature listed above remain unchanged: ion-neutral coupling would still cause horizontal plasma flow in the ionosphere, leading to unexpected magnetic field distributions.

Over the regions where the transition occurs from an impact-ionized-ram-side-ionosphere to a solar-illuminated-dayside-ionosphere, thermal pressure gradient forces align mainly from day to night while magnetic field pressure gradient forces aligns from night to day (Fig. 5). Therefore at around 1300 km (between 1000 and 1500 km) a transition region forms where the directions of these gradient forces oppose (Cravens et al., 2010). As also discussed in the previous section, over the flanks, dynamic pressure (ρv^2) is high due to acceleration of the plasma and high plasma density and thus comparable to thermal and magnetic pressures. This region is potentially turbulent and complex with the possibility of velocity shear related and other instabilities. At high altitudes above the ionosphere (above ~5000 km), dynamic pressure dominates due to the faster plasma flow. At these altitudes pressure gradient forces mainly align from night to day (Fig. 5), giving a more traditional plasma interaction picture.

6. Discussion of the magnetic field

We now analyze in some detail the possible reasons for the inconsistencies at low altitudes between measured ion densities and magnetic field and densities and field from the MHD simulation (Section 4). While the ion densities are well represented by the model, the magnetic field measurements are significantly different in direction from the model predictions within the ionosphere. Possible reasons for these inconsistencies include the application of ill-constrained model boundary conditions, uncertainties in the upstream parameters, temperature representations in the model, assumption of zero neutral velocity and limitations of the MHD theory, such as kinetic effects. The heavy ions such as the magnetospheric O^+ make a transition from primarily kinetic behavior above the exobase to a collisional description in the ionosphere. An ideal MHD model is not capable of including the results of this transition on the currents or the related magnetic fields. This may be one of the reasons for the discrepancies observed in the magnetic field calculations. Furthermore, time variations in the external magnetic field and the response of Titan's ionosphere to these variations may also cause unpredicted magnetic field distributions. Due to rather long time constants (in excess of an hour near 1200 km – Cravens et al., 2010), Titan's ionosphere may preserve magnetic field configurations that reflect external conditions (e.g., variations in Saturn's magnetospheric field at 20 Rs or passage through the magnetopause as during T32) from earlier times – (Wei et al., 2008; Bertucci et al., 2008; Neubauer et al., 2006). As our model assumes a constant upstream magnetic field, it does not account for such possible time variation effects. In addition to the external diffused field Cassini magnetometer may also measure a magnetic field whose origin is induction in surface or subsurface conducting material by a time-varying external field. In the presence of a conducting layer at the surface or below, a time-varying inducing field could generate an induced field that opposes the variation of the inducing field resulting in the magnetic field discrepancies observed for T5. This type of effect has been invoked to explain the magnetic field perturbations measured near some of the Galilean satellites (Kivelson et al., 1999; Khurana et al., 1998). In this section we examine three of the reasons listed above in more detail, including the model assumptions used in the magnetic field evolution, weaknesses in the plasma temperature representations and zero neutral velocity assumption.

In the MHD formulation, the magnetic field is calculated using Faraday's law (Eq. (6)) and the electric field is obtained from the Generalized Ohm's law (Eq. (7)).

$$\frac{\partial \mathbf{B}}{\partial t} = -\nabla \times \mathbf{E} \tag{6}$$

$$\mathbf{E} = -\mathbf{u} \times \mathbf{B} - \frac{\mathbf{J} \times \mathbf{B}}{ne} + \frac{\nabla p}{ne} + \eta \mathbf{J} + \frac{m_e}{n_e e} \frac{\partial \mathbf{J}}{\partial t} \tag{7}$$

$$\frac{\partial \mathbf{B}}{\partial t} \approx -\nabla \times \left[\mathbf{u} \times \mathbf{B} - \frac{\mathbf{J} \times \mathbf{B}}{ne} + \frac{\nabla p}{ne} + \eta \mathbf{J} \right] \tag{8}$$

In these equations **u** is plasma velocity, **B** is magnetic field, **J** is current density, n is electron density, e is electron charge, p is thermal pressure, and η is resistivity. In the magnetic induction equation (Eq. (8)), the first term is convective, the second term is Hall, the third term is polarization and the last term is the ohmic component of the magnetic field evolution. In the model calculations presented in this study, the Hall and polarization terms are ignored. However, in a weakly ionized ionosphere such as Titan's (electron–neutral density ratio is below 10^{-4} over the entire ionosphere), this approximation may not be appropriate. In addition, the Hall term can be ignored only when the gyrofrequency of the electrons is much less than the electron collision frequency. However, in Titan's ionosphere the electron gyrofrequency (~400 Hz) is much higher than the electron–neutral collision frequency above 900 km altitude.

In a recent study where the Hall effects were taken into account, Ma et al. (2007) also argued that the Hall term may be important in Titan's ionosphere even though the draping structure is not significantly affected by this term. In order to determine the relative importance of other components as well as the Hall term in the magnetic induction, we calculated their values along the T5 trajectory and plotted them in Fig. 9 even though this is not strictly self-consistent. Inbound and outbound components are shown on the first and the second panels respectively. As seen in this figure, the ohmic component only becomes important in the lower ionosphere below ~1000 km, which is consistent with Keller et al. (1994) and Cravens et al. (2010). However the polarization term is comparable to the convective and Hall component over the entire ionosphere, which is surprising as this term is expected to be important only over local regions, where the electron density and temperature gradients are not entirely parallel such as the terminator region (Cravens et al., 2010). One reason for the larger polarization term prediction may be a more varying temperature in the model calculations than the actual observations in the lower

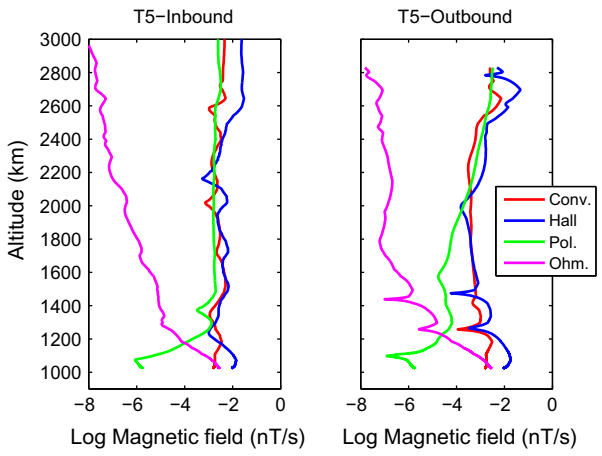

Fig. 9. Altitude profiles of the individual components in the generalized ohm's law, calculated from the model results along T5. Motional term is in red, Hall term is in blue, polarization term is in green and ohmic term is in magenta. The profiles are plotted along the inbound and outbound legs on the first and the second panels, respectively. (For interpretation of the references to color in this figure legend, the reader is referred to the web version of this article.)

ionosphere, yielding larger thermal pressure gradients (Eq. (7)). Using the same approach as Cravens et al., we calculated the contribution from these four components to the magnetic field within about a 10^4 s time interval and found that their contributions can reach 10 nT. This value is comparable to the ionospheric magnetic field measurements and consistent with the empirical predictions made by Cravens et al. (2010), which implies that the Hall and polarization terms may be important in Titan's ionosphere and the difference between the observed and calculated magnetic fields may be due to exclusion of these terms in the model calculations.

In Fig. 10, we compare magnetic field strength, thermal pressure and temperature obtained from the MHD model (blue dotted line) and from the Cassini observations (black solid line) (CAPs, MAG, LP) along the T5 trajectory outbound leg. As seen in these plots, the model underestimates the electron temperature and therefore the thermal pressures in the lower ionosphere. Weak thermal pressure at low altitudes makes the movement of the plasma, and therefore the convection and diffusion of the magnetic field, to lower altitudes slower in the model than in the real case, which may partially account for the larger magnetic field strengths predicted in the model. Although these results imply that a better electron temperature treatment would improve the model magnetic field predictions in the ionosphere, a recent update of the model with such treatment did not show significant differences in the ionospheric field distributions for all flybys (personal communication with Yingjuan Ma). This implies that other factors – such as time variations and neutral wind effects – may be more effective in determining the magnetic field structure in the lower ionosphere.

Another reason for the differences between the model and observed magnetic fields may be the exclusion of the possible coupling of the plasma and the neutral winds in the model. Although the neutral winds with considerable speeds from low to high latitudes and from day to night are expected to exist at Titan, the model assumes zero neutral winds (Müller-Wodarg et al., 2008). In the empirical thermospheric model of Muller-Wodarg et al., the horizontal components of these winds reach 150 m/s at high altitudes (~1800 km) (Müller-Wodarg et al., 2008) and ~100 m/s at around 1300 km altitude. In the model, these values are one order of magnitude less however, even these lower wind speeds are comparable to the bulk plasma velocity (tens of m/s) in the model and may cause strong horizontal drag forces (Section 5.2). If the collisions with the neutrals become frequent enough in the lower ionosphere, ionospheric plasma may move with the neutrals and magnetic field distributions may be greatly altered, causing the discrepancy between the measured and calculated magnetic fields. Moreover, as expected for T5 conditions (over the dawn region, Section 5), a shear formed between the oppositely directed neutral and plasma flows may also lead to unpredictable magnetic field distributions at low altitudes, below 1300 km, in Titan's ionosphere. More accurate descriptions of the ionospheric dynamics and understanding the role of the neutral winds in the overall dynamics require the inclusion of the neutral winds in future 3D MHD simulations.

7. Summary

In this paper, we analyzed a single-fluid multi-species 3D MHD simulation for the T5 flyby and compared the model calculations to the Cassini observations. The T5 flyby is unique in that it represents the particular case where the dayside and corotation ram side hemispheres are on opposite sides of Titan. We provided an in-depth analysis of the ionospheric force balance for this case, as well as providing a detailed discussion exploring the reasons for differences between the calculations and actual measurements for future modeling attempts. Our analysis results confirm the major key points from an empirical-along track analysis of Cravens et al. (2010), many of which are included in the conclusions listed below.

Comparison of the simulation results to Cassini observations during the T5 flyby show that

- Model ion densities fit well with the INMS and RPWS measurements while the model does not reproduce the measured ionospheric magnetic field very well.
- Unlike Venus' ram side ionosphere, there is no clear transition dominated by the evolution from external dynamic, to magnetic, to ionospheric thermal pressures in Titan's ram side ionosphere. On the corotation ram side and nightside, magnetic pressure dominates at low altitudes; the nightside thermal pressure is not enough to balance the dynamic pressure entirely. Magnetic resistivity becomes dominant at ~1000 km and the non-zero magnetic field in the lower ionosphere may

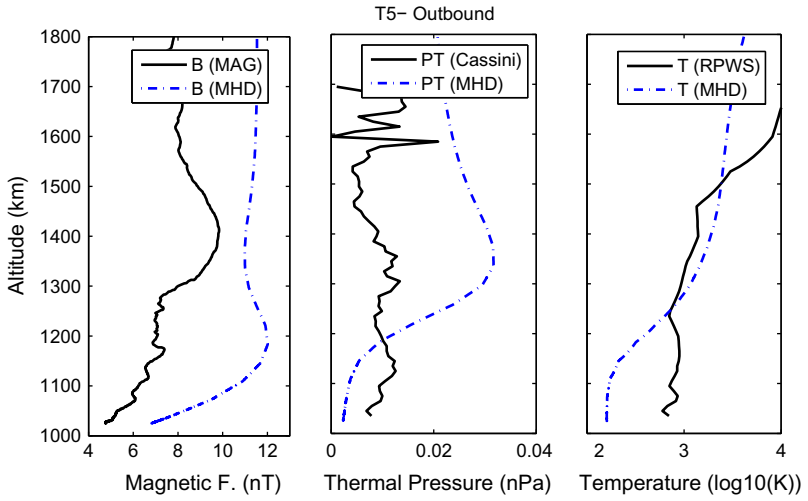

Fig. 10. Altitude profiles of the magnetic field, thermal pressure and temperature from the model calculations (dashed blue) and Cassini measurements (black) along T5 trajectory for the outbound leg (only outbound ion densities are available for T5). Magnetic fields are in nT, pressures are in nPa and temperatures are in K on a logarithmic scale. (For interpretation of the references to color in this figure legend, the reader is referred to the web version of this article.)

be due to penetration of the sub-flow magnetic barrier into the ionosphere by plasma convection down to 1000 km and due to magnetic diffusion below 1000 km altitude. While the ohmic term in the induction equation is important only in the deep ionosphere below ~1000 km, Hall and polarization terms may be important throughout the entire ionosphere of Titan.

- The drag force provides the force balance everywhere in the lower ionosphere and horizontal components of the drag forces are significant over the ram flanks, confirming that the Titan interaction is an inherently 3D problem. Neutral wind speeds at low altitudes are comparable to model plasma speeds, and so the estimated wind-related drag forces from the thermodynamic models (Müller-Wodarg et al., 2008) due to possible ion-neutral coupling is significant below ~1300 km altitude. The neutral wind and plasma drag forces are aligned in opposite directions leading a shear over the dawn/$-y$ flanks. Similarly the thermal and magnetic pressure gradients oppose at ~1300 km over the ram flanks leading a shear over these regions, altering the magnetic field in the ionosphere from the direction of the original penetrating field.
- Unlike Venus' nightside wake, Titan's ram wake is on the dayside for T5 and dominated by thermal ionospheric pressure extending to several Titan radii. There is not considerable cross-terminator plasma flow and the nightside ionosphere is mostly produced by magnetospheric plasma impact.

The main disagreement between the magnetic field measurements and the model results may be due to:

- Neutral wind effects and possible ion-neutral coupling below 1300 km, the "magnetic memory" feature of Titan's ionosphere, the induction generated at the surface or subsurface by a time-varying external field and/or Hall and polarization terms, all of which are ignored in the magnetic field calculation in the simulation. All these factors, including possible shear related instabilities, may lead to unpredictable magnetic field distributions in the ionosphere.
- The plasma temperature is not well predicted by the model at low altitudes, affecting the redistribution of the field by thermal pressure gradient forces. Other possible reasons are the application of inappropriate model boundary conditions, uncertainties in the upstream parameters or non-MHD effects.

The resolution of the issues described above needs to be addressed by future modeling efforts as well as similar careful diagnostic analysis of a number of further Titan flybys. Comprehensive model–data cross-body comparisons for Titan, Venus and Mars would help in determining the similarities or diversities in their ionospheric dynamics. Such a study is a future objective which we plan to address in a follow up paper.

Acknowledgments

D. Ulusen thanks D.A. Brain for useful discussions. This research was supported by NASA's Cassini project.

References

Agren, K., and 15 colleagues, 2007. On magnetospheric electron impact ionization and dynamics in Titan's ram-side and polar ionosphere - a Cassini case study. Annales Geophysicae 25(11), 2359-2369.

Agren, K., Wahlund, J.-E., Garnier, P., Modolo, R., Cui, J., Galand, M., Muller-Wodarg, I., 2009. On the ionospheric structure of Titan. Planet. Space Sci. 57 (14-15), 1821–1827.

Backes, H., and 10 colleagues, 2005. Titan's magnetic field signature during the first Cassini encounter. Science 308, 992–995.

Bertucci, C., and 11 colleagues, 2008. The magnetic memory of Titan's ionized atmosphere. Science 321 (5895), 1475–1478.

Bertucci, C., Sinclair, B., Achilleos, N., Hunt, P., Dougherty, M.K., Arridge, C.S., 2009. The variability of Titan's magnetic environment. Planet. Space Sci. (57), 1813–1820.

Bird, M.K., Dutta-Roy, R., Asmar, S.W., 1997. Detection of Titan's ionosphere from Voyager 1 radio occultation observations. Icarus 130 (2), 426–436.

Brace, L.H., Kliore, A.J., 1991. The structure of the Venus ionosphere. Space Sci. Rev., 81–163. ISSN 0038-6308.

Brace, L.H., Theis, R.F., Mihalov, J.D., 1990. Response of nightside ionosphere and ionotail of Venus to variations in solar EUV and solar wind dynamic pressure. J. Geophys. Res. 95 (1), 4075–4084. ISSN 0148-0227.

Brecht, S.H., Luhmann, J.G., Larson, D.J., 2000. Simulation of the saturnian magnetospheric interaction with Titan. J. Geophys. Res. 105 (13), 119.

Crary, F.J., Magee, B.A., Mandt, K., Waite, J.H., Westlake, J., Young, D.T., 2009. Heavy ions, temperatures and winds in Titan's ionosphere: Combined Cassini CAPS and INMS observations. Planet. Space Sci. 57 (14–15), 1847–1856.

Cravens, T.E., Crawford, S.L., Nagy, A.F., Gombosi, T.I., 1983. A two-dimensional model of the ionosphere of Venus. J. Geophys. Res. 88 (1), 5595–5606. ISSN 0148-0227.

Cravens, T.E., Lindgren, C.J., Ledvina, S.A., 1998. A two-dimensional multifluid MHD model of Titan's plasma environment. Planet. Space Sci. 46 (9–10), 1193–1205.

Cravens, T.E., and 15 colleagues, 2005. Titan's ionosphere: Model comparison with Cassini Ta data. Geophys. Res. Lett. 32 (12), L12108.

Cravens, T. E., and 14 colleagues, 2006. The composition of Titan's ionosphere. Geophys. Res. Lett. 33 (7); L07105.

Cravens, T.E., Robertson, I.P., Ledvina, S.A., Mitchell, D., Krimigis, S.M., Waite, J.H., 2008. Energetic ion precipitation at Titan. Geophys. Res. Lett. 35 (3), L03103.

Cravens, T.E., and 11 colleagues, 2009a. Model–data comparisons for Titan's nightside ionosphere. Icarus 199 (1), 174–188.

Cravens, T.E., Yelle, R.V., Wahlund, J.-E., Shemansky, D.E., Nagy, A.F., 2009b. Composition and Structure of the Ionosphere and Thermosphere. Titan from Cassini–Huygens by Springer Science (Chapter 11).

Cravens, T.E., and 14 colleagues, 2010. Dynamical and magnetic field time constants for Titan's ionosphere – Empirical estimates and comparisons with Venus. J. Geophys. Res.in press, doi:10.1029/2009JA015050.

Cui, J., Galand, M., Yelle, R.V., Vuitton, V., Wahlund, J.-E., Lavvas, P.P., Muller-Wodarg, I.C.F., Cravens, T.E., Kasprzak, W.T., Waite Jr., J.H., 2009. Diurnal variations of Titan's ionosphere. J. Geophys. Res. 114, A06310.

Dougherty, M. K., and 12 colleagues, 2004. The Cassini magnetic field investigation. Space Science Reviews, 114 (1-4), 331-383.

Elphic, R.C., Russell, C.T., Slavin, J.A., Brace, L.H., 1980. Observations of the dayside ionopause and ionosphere of Venus. J. Geophys. Res. 85 (December 30), 7679–7696.

Fox, J.L., Yelle, R.V., 1997. Hydrocarbon ions in the ionosphere of Titan. Geophys. Res. Lett. 24, 2179–2182.

Gan, L., Keller, C.N., Cravens, T.E., 1992. Electrons in the ionosphere of Titan. J. Geophys. Res. 97 (A8), 12137–12151.

Gurnett, D.A., and 29 colleagues, 2004. The Cassini Radio and Plasma Wave Investigation. Space Science Reviews 114(1-4), 395-463.

Hartle, R.E., Sittler Jr., E.C., Ogilvie, K.W., Scudder, J.D., Lazarus, A.J., Atreya, S.K., 1982. Titan's ion exosphere observed from Voyager 1. J. Geophys. Res. 87 (March 1), 1383–1394.

Ip, W.H., 1990. Titan's upper ionosphere. Astrophys. J. 362, 354–363.

Kabin, K., Gombosi, T.I., Dezeeuw, D.L., Powell, K.G., Israelevich, P.L., 1999. Interaction of the saturnian magnetosphere with Titan: Results of a there dimensional MHD simulation. J. Geophys. Res. 104 (A2), 2451–2458.

Kabin, K., Israelevich, P.L., Ershkovicj, A.I., Neubauer, F.M., Gombosi, T.I., DeZeeuw, D.L., Powell, K.G., 2000. Titan's magnetic wake: Atmospheric or magnetospheric interaction. J. Geophys. Res. 105 (A5), 10761–10770.

Keller, C.N., Cravens, T.E., 1994. One dimensional multispecies hydrodynamic models of the wakeside ionosphere of Titan. J. Geophys. Res. 99 (A4), 6527–6536.

Keller, C.N., Cravens, T.E., Gan, L., 1992. A model of the ionosphere of Titan. J. Geophys. Res. 97 (A8), 12117–12135.

Keller, C.N., Cravens, T.E., Gan, L., 1994. One dimensional multispecies magnetohydrodynamic models of the ramside ionosphere of Titan. J. Geophys. Res. 99 (A4), 6511–6525.

Keller, C.N., Anicich, V.G., Cravens, T.E., 1998. Model of Titan's ionosphere with detailed hydrocarbon chemistry. Planet. Space Sci. 46 (9–10), 1157–1174.

Khurana, K.K., Kivelson, M.G., Stevenson, D.J., Schubert, G., Russell, C.T., Walker, R.J., Polanskey, C., 1998. Induced magnetic fields as evidence for subsurface oceans in Europa and Callisto. Nature 395 (6704), 777–780.

Kivelson, M.G., Khurana, K.K., Stevenson, D.J., Bennett, L., Joy, S., Russell, C.T., Walker, R.J., Zimmer, C., Polanskey, C., 1999. Europa and Callisto: Induced or intrinsic fields in a periodically varying plasma environment. J. Geophys. Res. 104 (A3), 4609–4626.

Knudsen, W.C., Spenner, K., Miller, K.L., Novak, V., 1980. Transport of ionospheric O/+/ions across the Venus terminator and implications. J. Geophys. Res. 85 (December 30), 7803–7810.

Ledvina, S.A., Cravens, T.E., 1998. A three-dimensional MHD model of plasma flow around Titan. Planet. Space Sci. 46 (9–10), 1175–1191.

Luhmann, J.G., Cravens, T.E., 1991. Magnetic fields in the ionosphere of Venus. Space Sci. Rev. 55 (January–February), 201–274.

Luhmann, J.G., Phillips, J.L., Russell, C.T., 1987. Studies of the configuration of the Venus ionospheric magnetic field. Adv. Space Res. 7 (12), 101–106.

Ma, Y., Nagy, A.F., Cravens, T.E., Sokolov, I.G., Clark, J., Hansen, K.C., 2004a. 3-D global model prediction for the first close flyby of Titan by Cassini. Geophys. Res. Lett. 31, L22803.

Ma, Y., Nagy, A.F., Sokolov, I.V., Hansen, K.C., 2004b. Three dimensional, multispecies, high spatial resolution MHD studies of the solar wind interaction with Mars. J. Geophys. Res. 109, A07211.
Ma, Y.-J., Nagy, A.F., Cravens, T.E., Sokolov, I.U., Hansen, K.C., Wahlund, J.-E., Crary, F.J., Coates, A.J., Dougherty, M.K., 2006. Comparisons between MHD model calculations and observations of Cassini flybys of Titan. J. Geophys. Res. 111, A05207.
Ma, Y.-J., and 10 colleagues, 2007. 3D global multispecies Hall-MHD simulation of the Cassini T9 flyby. Geophys. Res. Lett. 34 (24), L24S10.
Magee, B.A., Waite, J.H., Mandt, K.E., Westlake, J., Bell, J., Gell, D.A., 2009. INMS-derived composition of Titan's upper atmosphere: Analysis methods and model comparison. Planet. Space Sci. 57 (14–15), 1895–1916.
Modolo, R., Chanteur, G.M., Wahlund, J.-E., Canu, P., Kurth, W.S., Gurnett, D., Matthews, A.P., Bertucci, C., 2007. Plasma environment in the wake of Titan from hybrid simulation: A case study. Geophys. Res. Lett. 34, L24S07.
Müller-Wodarg, I.C.F., Yelle, R.V., Cui, J., Waite, J.H., 2008. Horizontal structures and dynamics of Titan's thermosphere. J. Geophys. Res. 113, E10005.
Nagy, A.F., Cravens, T.E., 1998. Planet. Space Sci. 46 (9–10), 1149–1155.
Nagy, A.F., Liu, Y., Hansen, K., Kabin, K., Gombosi, T.I., Combi, M.R., DeZeeuw, D.L., Powell, K.G., Kliore, A.J., 2001. The interaction between the magnetosphere of Saturn and Titan's ionosphere. J. Geophys. Res. 106 (A4), 6151–6160.
Ness, N.F., Acuna, M.H., Behannon, K.W., Neubauer, F.M., 1982. The induced magnetosphere of Titan. J. Geophys. Res. 87, 1369–1381.
Neubauer, F.M., and 16 colleagues, 2006. Titan's near magnetotail from magnetic field and electron plasma observations and modeling: Cassini flybys TA, TB, and T3. J. Geophys. Res. 111 (A10) (CiteID A10220).
Powell, K.G., Roe, L., Linde, T.J., Gombosi, T.I., De Zeeuw, D.L., 1999. A solution adaptive upwind scheme for ideal magnetohyrodynamics. J. Comput. Phys. 154, 284–309.
Robertson, I.P., and 11 colleagues, 2009. Structure of Titan's ionosphere: Model comparisons with Cassini data. Planet. Space Sci. 57 (14–15), 1834–1846.
Rymer, A.M., Smith, H.T., Wellbrock, A., Coates, A.J., Young, Y.T., 2009. Discrete classification and electron energy spectra of Titan's varied magnetospheric environment. Geophys. Res. Lett. 36 (15).
Schunk, R.W., Nagy, A.F., 2000. Ionospheres: Physics, plasma physics, and chemistry. In: Dressler, A.J., Houghton, J.T., Rycroft, M.J. (Eds.), Cambridge Atmos. Space Sci. Ser. Cambridge Univ. Press, Cambridge, UK.
Shinagawa, H., Cravens, T.E., 1988. A one-dimensional multispecies magnetohydrodynamic model of the dayside ionosphere of Venus. J. Geophys. Res. 93 (October 1), 11263–11277. ISSN 0148-0227.
Simon, S., Motschmann, U., 2009. Titan's induced magnetosphere under non-ideal upstream conditions: 3D multi-species hybrid simulations. Planet. Space Sci. 57, 2001–2015.
Simon, S., Boesswetter, A., Bagdonat, T., Motschmann, U., Glassmeier, K.H., 2006. Plasma environment of Titan: A 3-d hybrid simulation study. Ann. Geophys. 24 (3), 1113–1135.
Simon, S., Wennmachera, A., Neubauer, F.M., Bertucci, C.L., Kriegel, H., Saur, J., Russell, C.T., Dougherty, M.K., 2010. Titan's highly dynamic magnetic environment: A systematic survey of Cassini magnetometer observations from flybys TA–T62. Planet. Space Sci. 58 (10), 1230–1251.
Sittler, E.C., Hartle, R.E., Bertucci, C., Coates, A., Cravens, T.E., Dandouras, I., Shemansky, D., 2009. Energy Deposition Processes in Titan's Upper Atmosphere and its Induced Magnetosphere. Titan from Cassini–Huygens by Springer Science (Chapter 16).
Wahlund, J.-E., and 17 colleagues, 2005. Cassini Measurements of Cold Plasma in the Ionosphere of Titan. S c i e n c e 308(5724), 986-989.
Waite, and 15 colleagues, 2004. The Cassini Ion and Neutral Mass Spectrometer (INMS) Investigation. Space Science Reviews 114(1-4), 113-231.
Waite, Jr. J.H., and 21 colleagues, 2005. Ion Neutral Mass Spectrometer (INMS) results from the first flyby of Titan. Science 308 (5724), 982–986.
Wei, H., Russell, C., Dougherty, M., Ma, Y., Hansen, K., McAndrews, H., Hospodarsky, G., Thomsenm, M., Young, D., 2008. American Geophysical Union, Fall Meeting, (abstract #P21A-1339).
Yung, Y.L., 1987. An update of nitrile photochemistry on Titan. Icarus 72 (November), 468–472.
Yung, Y.L., Allen, M., Pinto, J.P., 1984. Photochemisrty of the atmosphere of titan: Comparison between model and observations. Astrophys. J. 55 (July), 465–506.
Zhang, T.L., Luhmann, J.G., Russell, C.T., 1991. The magnetic barrier at Venus. J. Geophys. Res. 96 (July 1), 11145–11153. ISSN 0148-0227.
Zhang, T. L., and 26 colleagues, 2006. Magnetic field investigation of the Venus plasma environment: Expected new results from Venus Express, Planet. Space Sci. 54 (13-14), 1336-1343.
Zhang, T. L., and 28 colleagues, 2007. Little or no solar wind enters Venus' atmosphere at solar minimum, Nature 450 (7170), 654-656.